

Supporting information

Self-assembly of a supramolecular spin-crossover tetrahedron

Hannah H. Nielsen,^{a, c} Pol Vilariño,^a Gemma Rodríguez,^a Florian Trepard,^a Olivier Roubeau,^{*d} Guillem Aromí,^{*a, b} David Aguilà,^{*a, b}

^a *Departament de Química Inorgànica i Orgànica, Secció de Química Inorgànica, Universitat de Barcelona, Diagonal 645, 08028 Barcelona (Spain)*

^b *Institute of Nanoscience and Nanotechnology, University of Barcelona (IN2UB), 08007 Barcelona (Spain)*

^c *Department of Chemistry, Aarhus University, DK-8000 Aarhus (Denmark)*

^d *Instituto de Nanociencia y Materiales de Aragón (INMA), CSIC and Universidad de Zaragoza, Plaza San Francisco s/n, 50009, Zaragoza (Spain)*

Experimental Details.

Syntheses.

All reagents were purchased from commercial sources and used as received. HL was synthesized based on the synthesis of previously reported ligands.¹ TMA[FeCl₄] was obtained following the reported synthetic procedure.² Coordination chemistry reactions were carried out under aerobic conditions.

1-(pyridin-2-yl)-3-(pyridin-3-yl)propane-1,3-dione. Metallic sodium (0.36 g, 16 mmol) was suspended under nitrogen atmosphere in ethanol (10 mL) and stirred until all had reacted, leading to a cloudy suspension. To this mixture, a solution of 3-acetylpyridine (0.74 mL, 6.7 mmol) in diethyl ether (50 mL) was added dropwise, producing a pale-yellow solution. The latter was stirred for 10 minutes, and treated dropwise with a solution of ethyl-2-picolinate (0.89 mL, 6.6 mmol). The resulting green suspension was brought to reflux for 4 h. The system was then allowed to reach room temperature and a brownish solid was collected by filtration. This solid was suspended in H₂O (20 mL) and, to this suspension, acetic acid was added until a pH value of 3-4 was reached. After 15 minutes stirring, the product was isolated by filtration and washed several times with H₂O and dried in air. The yield was 70 % (in average). ¹H RMN (CD₃OD, 400MHz, ppm): 9.20 (s, 1H), 8.74 (m, 2H), 8.47 (d, 1H), 8.20 (d, 1H), 8.01 (t, 1H), 7.61 (m, 3H). MALDI-TOF: $m/z = 227.1$ ([M+H]⁺).

2-(5-(pyridin-3-yl)-1H-pyrazol-3-yl)pyridine (HL). 1-(pyridin-2-yl)-3-(pyridin-3-yl)propane-1,3-dione (1.04 g, 4.6 mmol) were suspended in MeOH (35 mL) and treated with N₂H₄·H₂O (360 μL, 4.83 mmol). The resulting solution was brought to reflux for 3 h, and then allowed to reach room temperature. The solution was concentrated almost to dryness, and the resulting solid of HL was collected by filtration and dried with diethyl ether. The yield was 80 % (in average). ¹H RMN (CD₃OD, 400MHz, ppm): 9.03 (br, 1H), 8.62 (br, 1H), 8.51 (br, 1H), 8.28 (br, 1H), 7.89 (m, 2H), 7.52 (t, 1H), 7.37 (q, 1H), 7.32 (s, 1H). Elemental analysis calcd (found) for HL·0.8H₂O: C 65.22 (65.98), H 4.07 (4.94), N 23.32 (23.67). MALDI-TOF: $m/z = 223.1$ ([HL+H]⁺).

[Fe(HL)₃](BF₄)₂ (1). A colorless solution of HL (30 mg, 0.135 mmol) in acetonitrile (10 mL) was added dropwise on a colorless solution of Fe(BF₄)·6H₂O (15 mg, 0.045 mmol) in acetonitrile (10 mL). Ascorbic acid (≈ 3 mg) was added on the resulting reddish solution and left stirring for 30 min. The solution was then filtered and layered with diethyl ether. Orange crystals were obtained after 3 weeks in 7 % yield (in average). IR: $\tilde{\nu} = 1734$ (mb), 1606 (m), 1570 (m), 1529 (w), 1484 (w), 1446 (s), 1340 (w), 1309 (w), 1259 (w), 1194 (w), 1048 (s), 1025 (s), 988 (s), 811 (w), 779 (s), 734 (w), 704 (s), 634 (w), 519 (m). Elemental analysis calcd (found) for 1·4H₂O: C 48.38 (48.93), H 3.96 (3.92), N 17.36 (17.46).

[FeCl₄]@{[Fe(HL)₃]₄}[FeCl₄]_{0.5}(BF₄)_{6.5}·(C₃H₆O)_{11.5} (2). A colorless solution of HL (40 mg, 0.18 mmol) in acetone (10 mL) was added dropwise on a colorless solution of Fe(BF₄)·6H₂O (20 mg, 0.06 mmol) in acetone (10 mL). The resulting reddish solution and

left stirring for 10 min and treated with a yellow solution of TMA[FeCl₄] (8.2 mg, 0.03 mmol) in acetone (3 mL). The solution, which turned orange, was stirred for 1 h and filtered, removing an orange solid. The orange filtrate was layered with diethyl ether, keeping it at 3 °C. Red crystals were obtained after one week in a 5 % yield (in average). IR: $\tilde{\nu}$ = 1704 (w), 1604 (m), 1569 (m), 1529 (w), 1492 (w), 1444 (s), 1408 (m), 1337 (w), 1307 (w), 1255 (w), 1192 (w), 1025 (s), 990 (s), 949 (s), 814 (w), 779 (s), 734 (w), 704 (s), 631 (w), 519 (m). Elemental analysis calcd (found) for **2**·(-10.2C₃H₆O)·28.9H₂O: C 44.18 (43.96), H 4.30 (4.06), N 15.48 (15.24).

Physical Characterization

Magnetic measurements. Direct current (*dc*) measurements were performed with either a MPMS-XL or MPMS3 SQUID magnetometers hosted by the Physical Measurements Unit of the Servicio General de Apoyo a la Investigación-SAI, Universidad de Zaragoza. The data were corrected for the contribution of the capsule sample holder, determined empirically. The sample diamagnetic contributions to the susceptibility were corrected using Pascal's constant tables. Measurements on compound **1** were done with the MPMS3 magnetometer. A first cycle was done using DC measurements and settling the temperature. The following thermal scans were done using VSM measurements at various temperature sweep rates, namely 5, 10, 20 and 3 K/min in this order. The same sample was measured again after two months kept at ambient conditions in its non-hermetic sample holder, and again on the same day after 3 hours kept at ambient conditions. A second set of measurements was performed on a second fresh batch, again with a first cycle done using DC measurements and settling the temperature, and further thermal scans done using VSM measurements at 3 K/min temperature sweep rates.

Differential Scanning Calorimetry (DSC). Differential Scanning Calorimetry (DSC) was used to obtain heat capacity in the range 120-450 K. Measurements were done with a Q1000 calorimeter from TA Instruments equipped with the LNCS accessory. The temperature and enthalpy scales were calibrated using a standard sample of In, through its melting transition (156.6 °C, 3296 Jmol⁻¹). Mechanically crimped Al pans with an empty pan as a reference were used. Data were obtained at a scanning rate of 10 Kmin⁻¹. Measurements of a sapphire reference sample under the same conditions were used to correct the obtained values of heat capacity.

Powder X-ray diffraction (PXRD). Measurements were done through the Servicio General de Apoyo a la Investigación, SAI-Universidad de Zaragoza, using a RIGAKU Ru2500 diffractometer with a rotating Cu anode and graphite monochromator to select Cu K α wavelength.

Mass Spectrometry. MALDI-TOF mass spectrometry measurements were performed on a 400 ABSciex MALDI-TOF spectrometer at the Unitat d'Espectrometria de Masses de Caracterització Molecular (CCiT) of the University of Barcelona. Solids were dissolved in

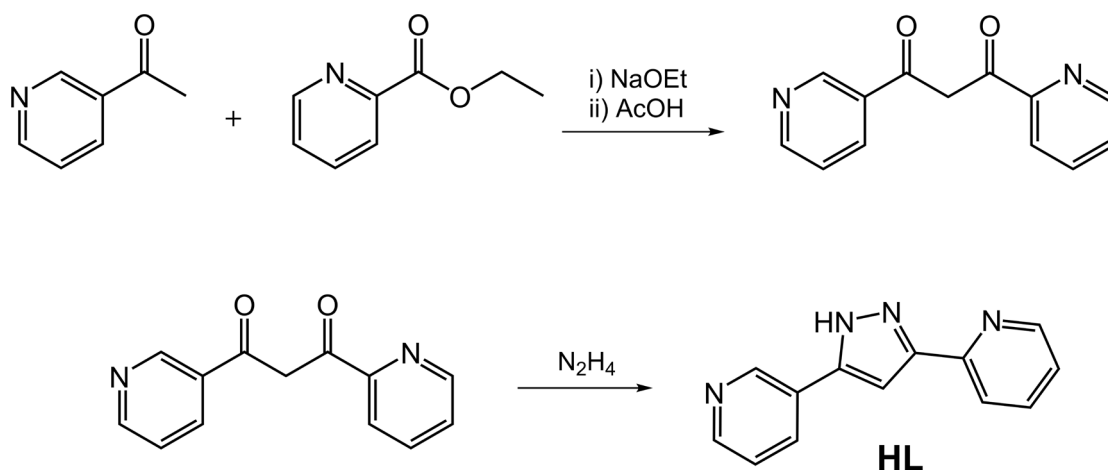
MeOH. Then, 0.5 μL of an internal reference solution, containing 10 mg/mL of DCTB in dichloromethane, was added before injection.

Elemental Analysis. C, H, N analyses were performed by using a Perkin-Elmer II Series CHNS/O equipment at the Microanalysis Service of the Institute for Advanced Chemistry of Catalonia.

Thermogravimetric analysis. Measurements were done at 5 $^{\circ}\text{C}/\text{min}$ under air using a TA Instruments 5000IR through the Thermal Analysis Service at INMA.

Single-Crystal X-Ray Diffraction. Data for compound **1** were collected on an orange plate at the BL13-XALOC beamline³ of the ALBA synchrotron ($\lambda = 0.72931 \text{ \AA}$) at 100 and 280 K. The crystal was mounted with Paratone N grease on a MiTegen kapton loop and placed in the N_2 stream of an Oxford Cryosystems Cryostream. A second crystal was evaluated following a thermal cycle. The crystal was introduced and collected at 300 K, then cooled down to 100 K (5 K/min) and collected again. The same crystal was then warmed up to 300 K (5 K/min) and collected. The structures were solved by intrinsic phasing with SHELXT⁴ and refined by full-matrix least-squares on F^2 with SHELXL.⁵ Data for compound **2** were obtained on a red block crystal of dimensions 0.140 x 0.130 x 0.072 mm³ at Beamline 12.2.1 of the Advanced Light Source (Berkeley, USA), on a Bruker D8 diffractometer equipped with a PHOTON II detector and using silicon (111) monochromated synchrotron radiation ($\lambda = 0.7288 \text{ \AA}$). The crystal was mounted from its mother solution with little apiezon N grease and protected from ambient atmosphere using a Mitegen polyester tube with solvent, to prevent loss of lattice solvent. The crystal was first measured at 275 K, then 300, 200 and 100 K. Data reduction and absorption corrections were performed with SAINT and SADABS, respectively.⁶ The structures were solved by intrinsic phasing with SHELXT⁴ and refined by full-matrix least-squares on F^2 with SHELXL.⁵ A fraction of the lattice acetone molecules were too diffuse to be refined (1, 11, 15 and 21 out of 23, respectively at 100, 200, 275 and 300 K), and the corresponding void spaces were analyzed and taken into account with PLATON/SQUEEZE.⁷ Possibly due to the process of localization of these diffuse molecules upon cooling, two of the Fe(II) complexes are disordered over two positions in the 100 and 200 K structures. All details can be found in CCDC 2334712-2334713 (for compound **1** at 100-280 K), CCDC 2353505-2353506-2353507 (for compound **1** at 300-100-300 K) and 2334714-2334715-2334716-2334717 (for compound **2** at 100-200-275-300 K) that contain the supplementary crystallographic data for this paper. These data can be obtained free of charge from The Cambridge Crystallographic Data Center via <https://summary.ccdc.cam.ac.uk/structure-summary-form>. Crystallographic and refinement parameters are summarized in Tables S1 and S2. Details of hydrogen bonds involved in the supramolecular $[\text{Fe}_4]$ tetrahedron in **2** and of the coordination environment of the Fe(II) ions are given in Tables S2 and S3 respectively.

¹H NMR Spectroscopy. ¹H NMR spectra were recorded with a Varian Mercury (400 MHz) instrument. Chemical shifts are reported in δ (parts per million) relative to an internal standard of tetramethylsilane or using the residual proteo solvent as internal reference.



Scheme S1. Chemical reaction of ligand HL.

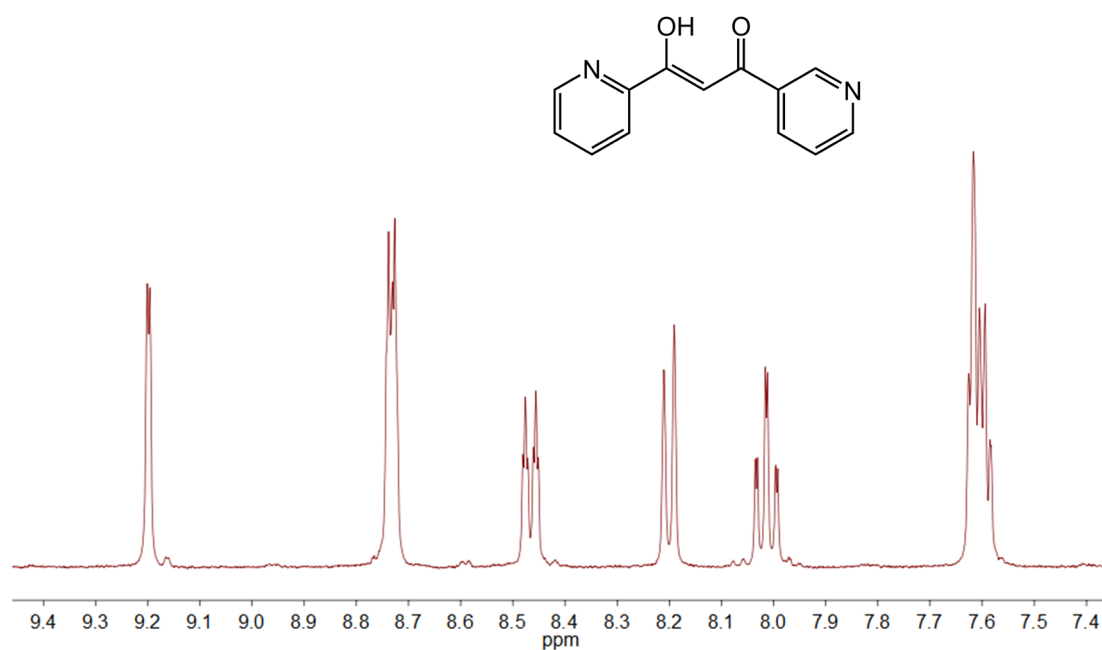


Figure S1. ^1H NMR spectrum of 1-(pyridin-2-yl)-3-(pyridin-3-yl)propane-1,3-dione.

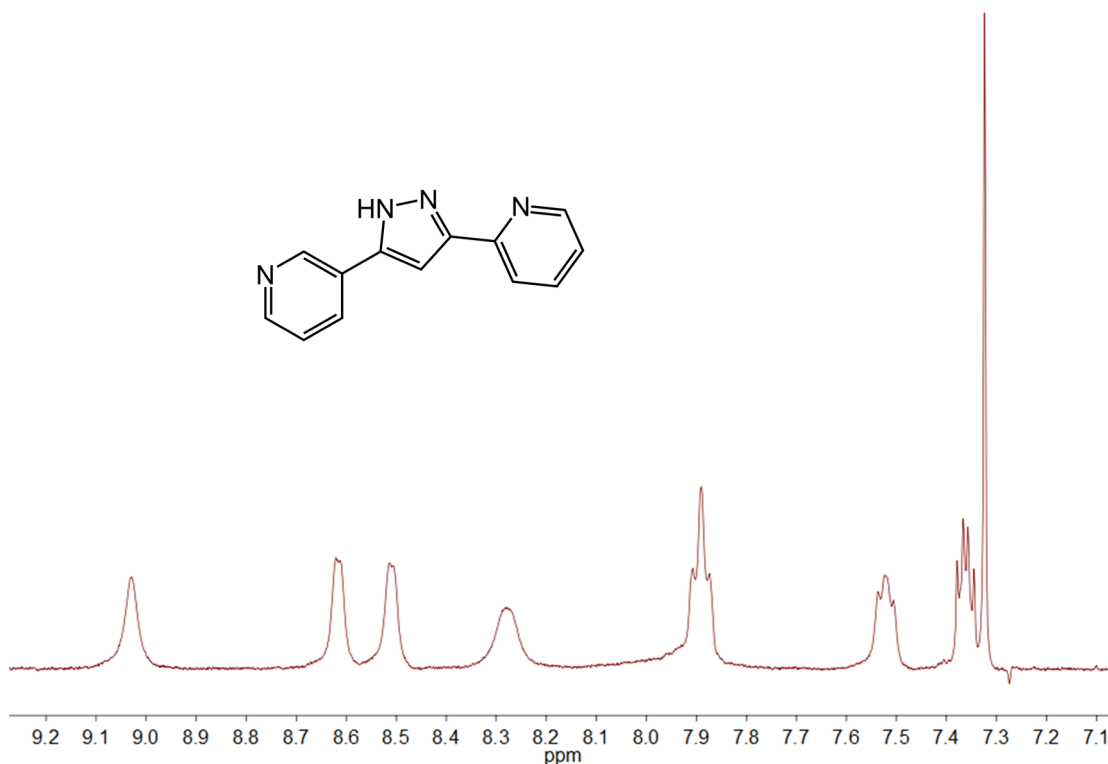


Figure S2. ^1H NMR spectrum of 2-(5-(pyridin-3-yl)-1H-pyrazol-3-yl)pyridine (HL).

Table S1. Crystallographic and refinement parameters for the structures of compound **1**.

T (K)	100	280	300	100	300
Formula	$\text{C}_{39}\text{H}_{30}\text{FeN}_{12}, 2(\text{BF}_4)$				
FW (g mol^{-1})	896.22				
Wavelength (\AA)	0.72932				
Crystal system	trigonal				
Space group	$P-3$				
a (\AA)	15.005(2)	15.172(2)	15.1758(5)	15.0044(8)	15.1790(4)
b (\AA)	15.005(2)	15.172(2)	15.1758(5)	15.0044(8)	15.1790(4)

c (Å)	10.863(2)	11.087(2)	11.1731(5)	10.9173(9)	11.1228(5)
α (°)			90		
β (°)			90		
γ (°)			120		
V (Å ³)	2118.1(7)	2210.2(8)	2228.47(18)	2128.5(3)	2219.38(15)
Z			2		
ρ_{calcd} (g cm ⁻³)	1.405	1.347	1.336	1.398	1.341
μ (mm ⁻¹)	0.464	0.445	0.440	0.461	0.442
indep. reflns. (R_{int})	4790 (0.1031)	3309 (0.0285)	2293 (0.0390)	2337 (0.0499)	1719 (0.0433)
parameters / restraints	220/42	220/40	220/40	220/40	220/40
GOF on F^2	1.087	1.052	1.086	1.132	1.106
R_1/wR_2 [$I > 2\sigma(I)$]	0.0826 / 0.2507	0.0706 / 0.2236	0.0686 / 0.2306	0.0629 / 0.2143	0.0705 / 0.2276
R_1/wR_2 (all data)	0.0854 / 0.2629	0.0728 / 0.2312	0.0729 / 0.2405	0.0675 / 0.2240	0.0741 / 0.2376
largest diff. peak / hole (e Å ⁻³)	0.916 / -1.583	0.574 / -0.419	0.541 / -0.252	0.556 / -0.367	0.416 / -0.245

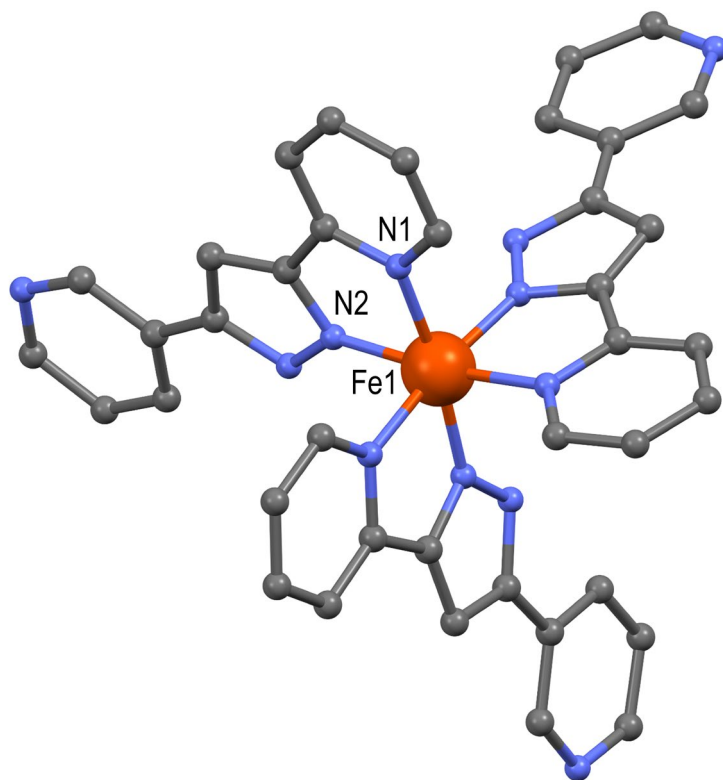


Figure S3. Representation of the $[\text{Fe}(\text{HL})_3]^{2+}$ cationic unit of **1**. Fe, N, C and H atoms are shown in orange, blue, grey and white, respectively.

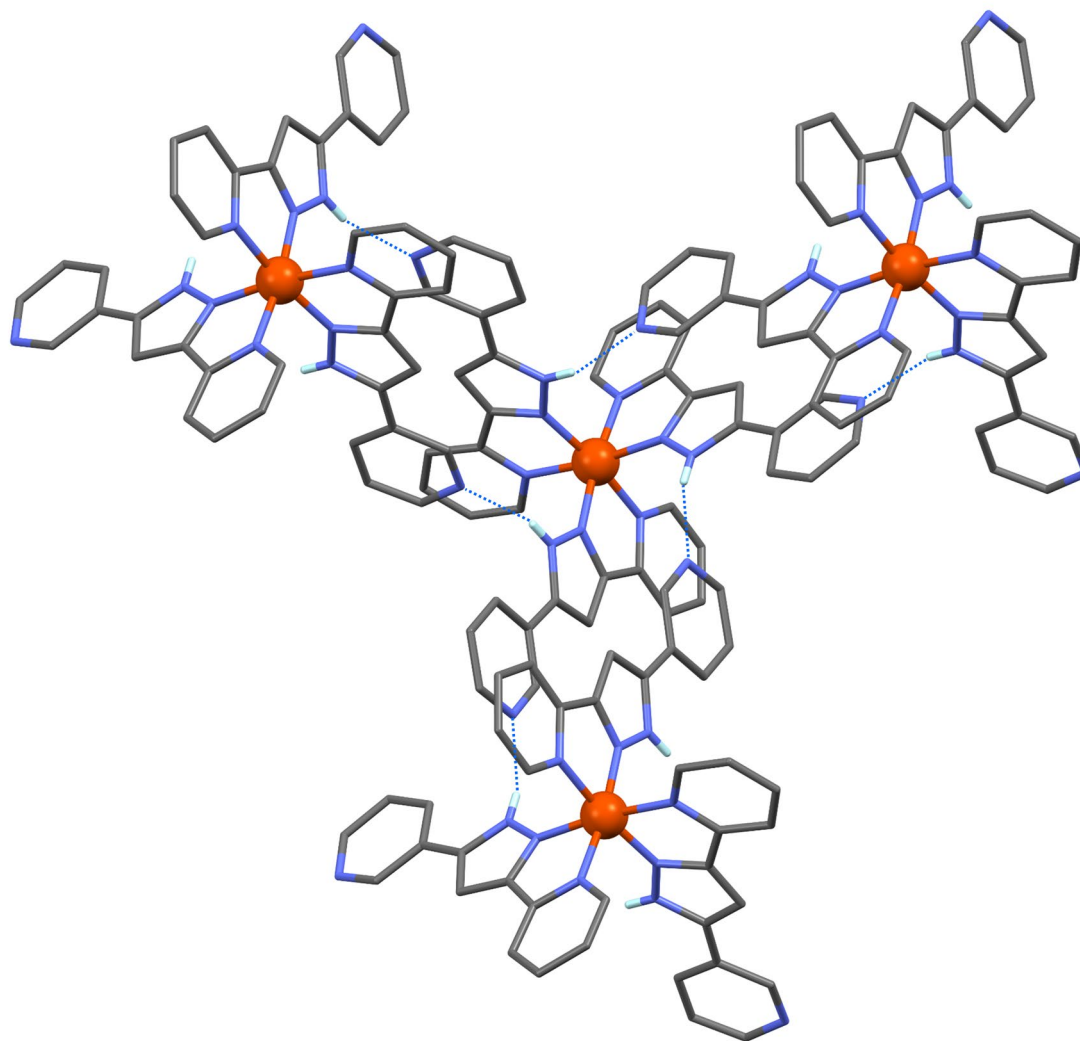


Figure S4. Representation of the crystal packing of compound **1** $[\text{Fe}(\text{HL})_3](\text{BF}_4)_2$ along the c axis, evidencing the H-bonding interactions (dashed blue lines) between the cationic iron units. Fe, N, C and H atoms are shown in orange, blue, grey, and white, respectively. Only H atoms from pyrazolyl NH group are shown for clarity.

Table S2. Selected hydrogen bonding in compound **1** $[\text{Fe}(\text{HL})_3](\text{BF}_4)_2$ at 100 and 280 K.

D–H⋯A	D–H (Å)	H⋯A (Å)	D⋯A (Å)	D–H⋯A (°)
100 K				
N3–H3⋯N4	0.87(5)	1.96(5)	2.755(3)	153(4)
280 K				
N3–H3⋯N4	0.89(5)	1.91(5)	2.783(4)	165(4)

Table S3. Selected interatomic distances (Å), angles (°) of compound **1** [Fe(HL)₃](BF₄)₂ at 100 and 280 K.

	100 K	280 K	300 K	100 K	300 K
Fe1 N1	2.0035(17)	2.136(2)	2.170(3)	2.012(3)	2.163(4)
Fe1 N2	1.9671(15)	2.0825(18)	2.105(3)	1.970(3)	2.109(3)
N2 Fe1 N2	96.08(6)	97.19(7)	97.52(10)	96.12(10)	97.41(12)
N2 Fe1 N1	172.81(6)	169.60(8)	168.75(11)	172.87(10)	169.02(13)
N2 Fe1 N1	80.20(7)	76.90(8)	75.97(12)	80.13(11)	76.05(14)
N2 Fe1 N1	90.45(7)	92.08(8)	92.47(11)	90.33(11)	92.22(13)
N1 Fe1 N1	93.62(7)	94.62(8)	94.95(12)	93.78(11)	95.19(13)

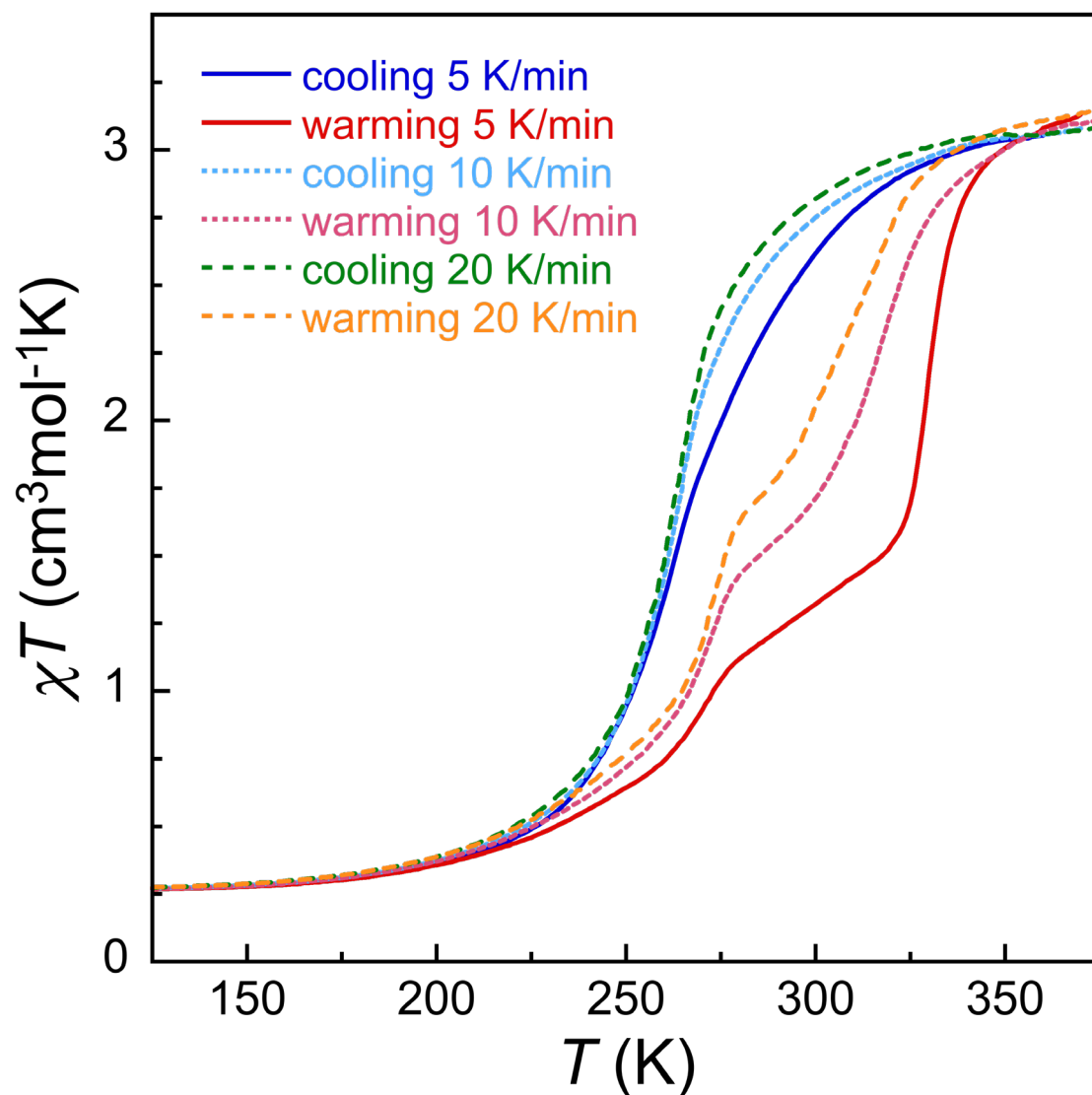


Figure S5. Effect of temperature scan-rate. Variable temperature dc magnetic susceptibility ($\chi = M/H$ per mole of compound) data for **1** collected under an applied field of 0.5 T. After a first cooling and heating cycle (see Fig. S6), four further thermal scans were successively at 5, 10, 20 and 3 K/min scan rates. The final cycle at 3 K/min is shown in Figure 2 of the manuscript. These data show the influence of the scan rate on the hysteretic behavior, although successive thermal cycling has an effect, as shown in Figure S11 through two successive thermal scans at the same scan rate for a second batch of **1**.

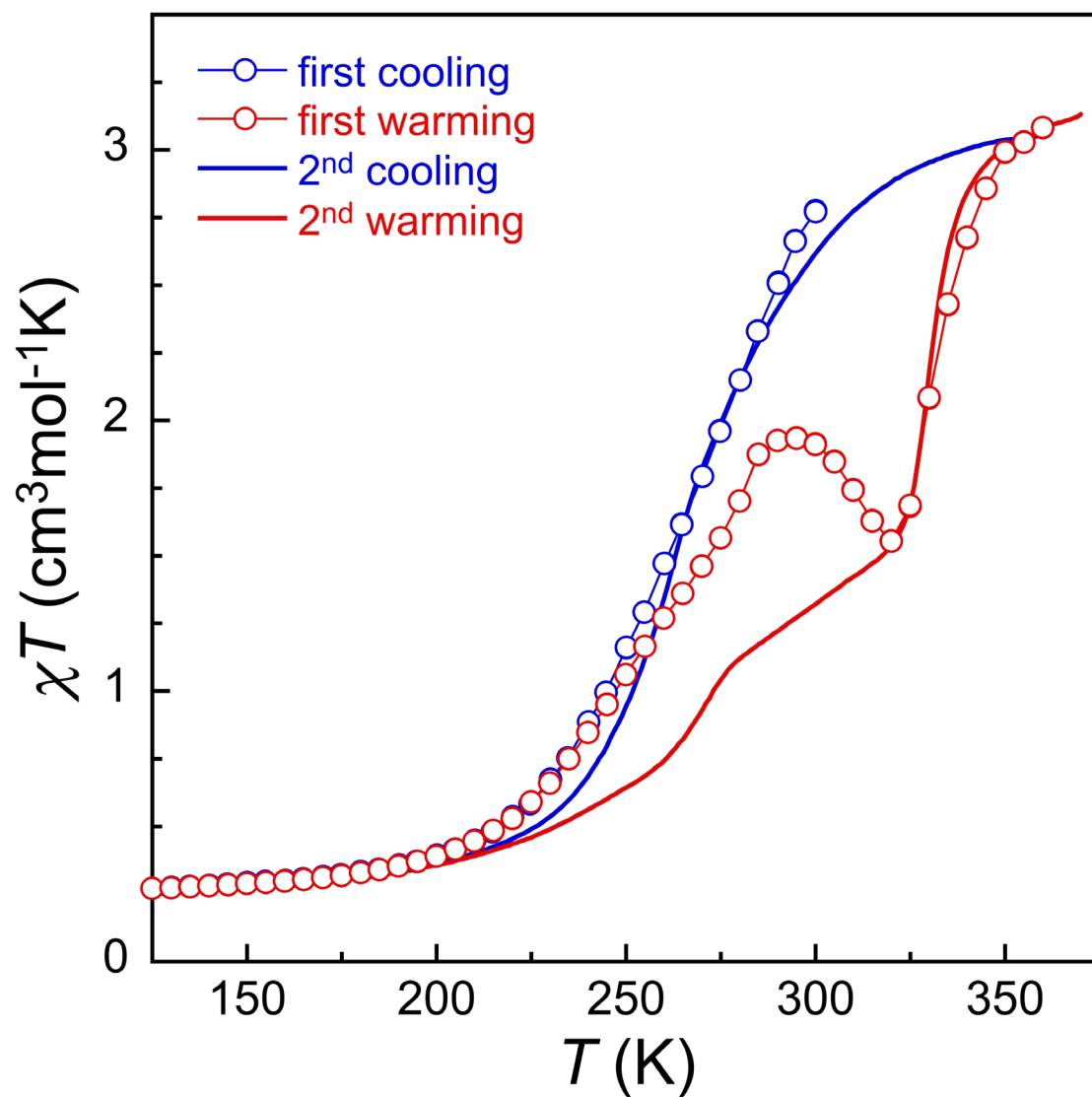


Figure S6. First thermal cycle. Variable temperature dc magnetic susceptibility ($\chi = M/H$ per mole of compound) data for **1** collected under an applied field of 0.5 T, showing the first cooling and heating cycle (symbols+lines, settle mode *ca.* 1 K/min) and the following second thermal cycle (thick lines, sweep mode, 5 K/min).

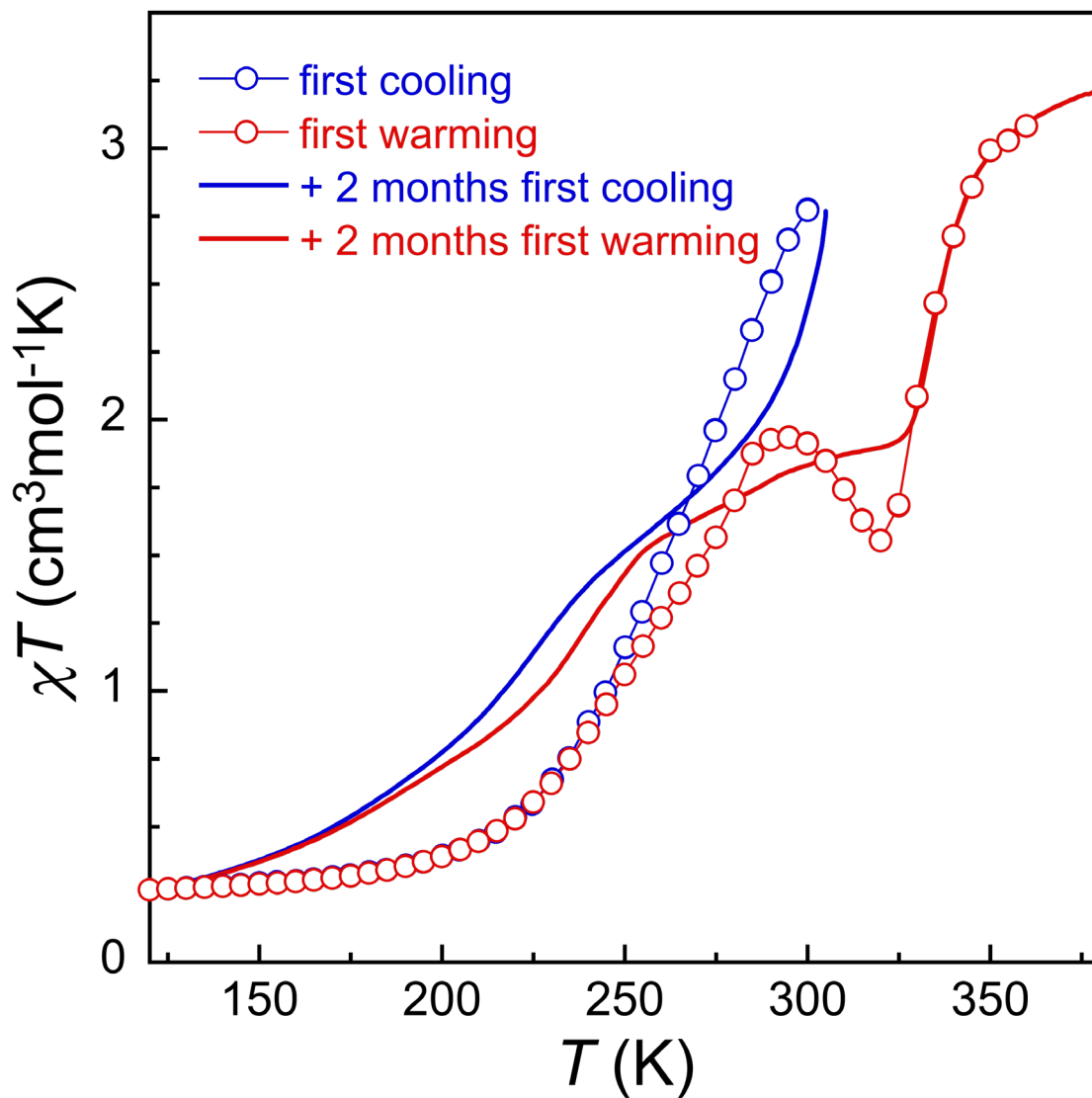


Figure S7. Effect of ageing. Variable temperature dc magnetic susceptibility ($\chi = M/H$ per mole of compound) data for **1** collected under an applied field of 0.5 T, comparing the original first cooling and heating cycles (symbols+lines) and the same measurement done on the same sample after 2 months under ambient conditions (lines).

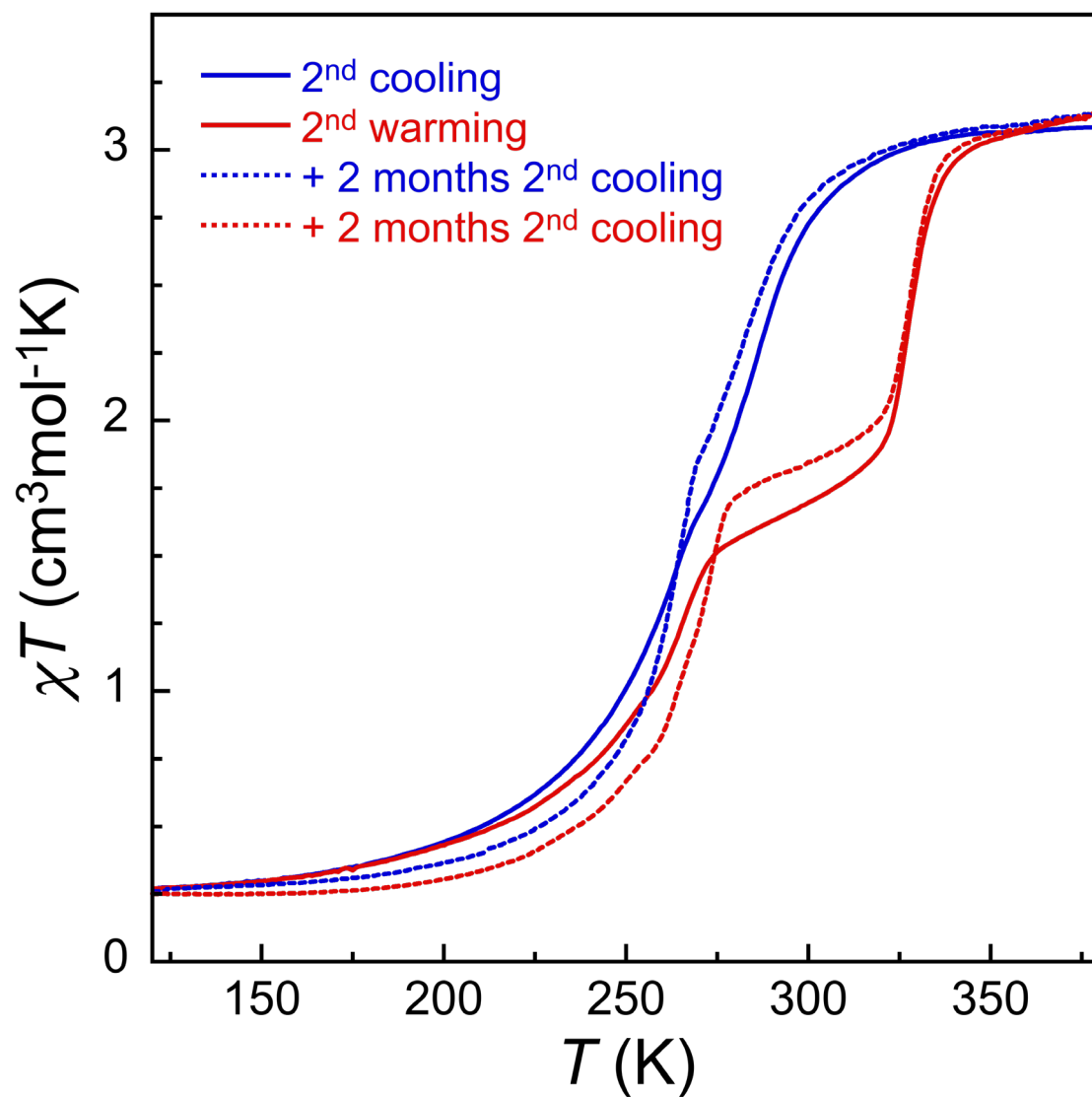


Figure S8. Reproducibility of SCO after warming to 380 K. Variable temperature dc magnetic susceptibility ($\chi = M/H$ per mole of compound) data for **1** collected under an applied field of 0.5 T, comparing the original second thermal scan and the same measurement done on the same sample after 2 months under ambient conditions, as indicated.

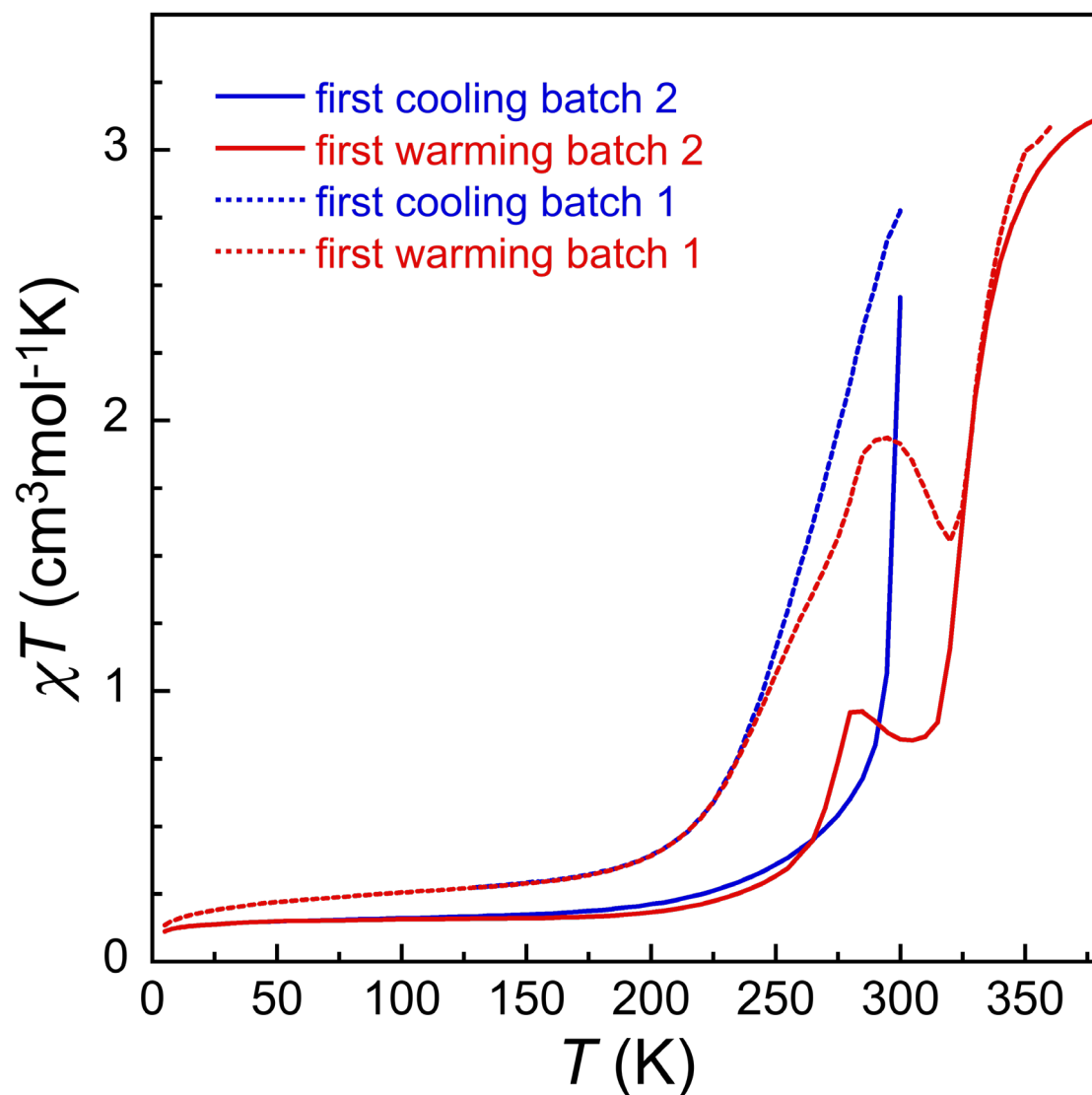


Figure S9. Batch to batch reproducibility of first cycle. Variable temperature dc magnetic susceptibility ($\chi = M/H$ per mole of compound) data collected under an applied field of 0.5 T, showing the first cooling and heating cycle for two different batches of **1**, as indicated. Note that the first batch had been standing under ambient conditions for several weeks before measurements, while the second one was measured “fresh”, *i.e.* less than a week after synthesis. This likely explains the differences in the abruptness of the cooling curve and in the height of the upturn observed at *ca.* 285 K upon warming.

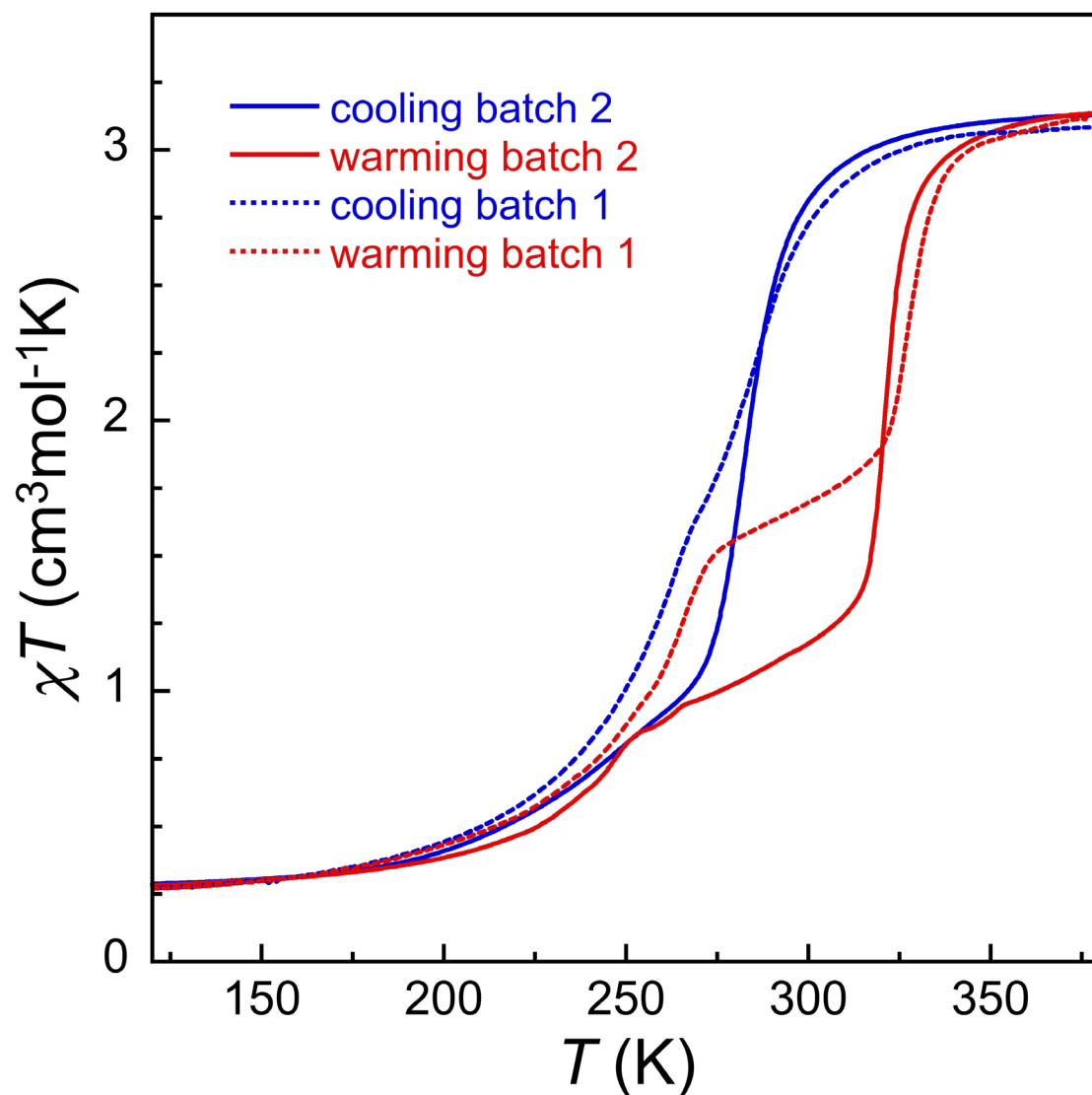


Figure S10. Batch to batch reproducibility of SCO after warming to 380 K. Variable temperature dc magnetic susceptibility ($\chi = M/H$ per mole of compound) data collected under an applied field of 0.5 T at 3 K/min for two different batches of **1**, as indicated. Note that the measurements for the first batch corresponds to a fifth thermal scan while that for the second batch is the second thermal scan. This likely partly explains the differences in the height of the plateau observed upon warming (see Fig. S8 and S11).

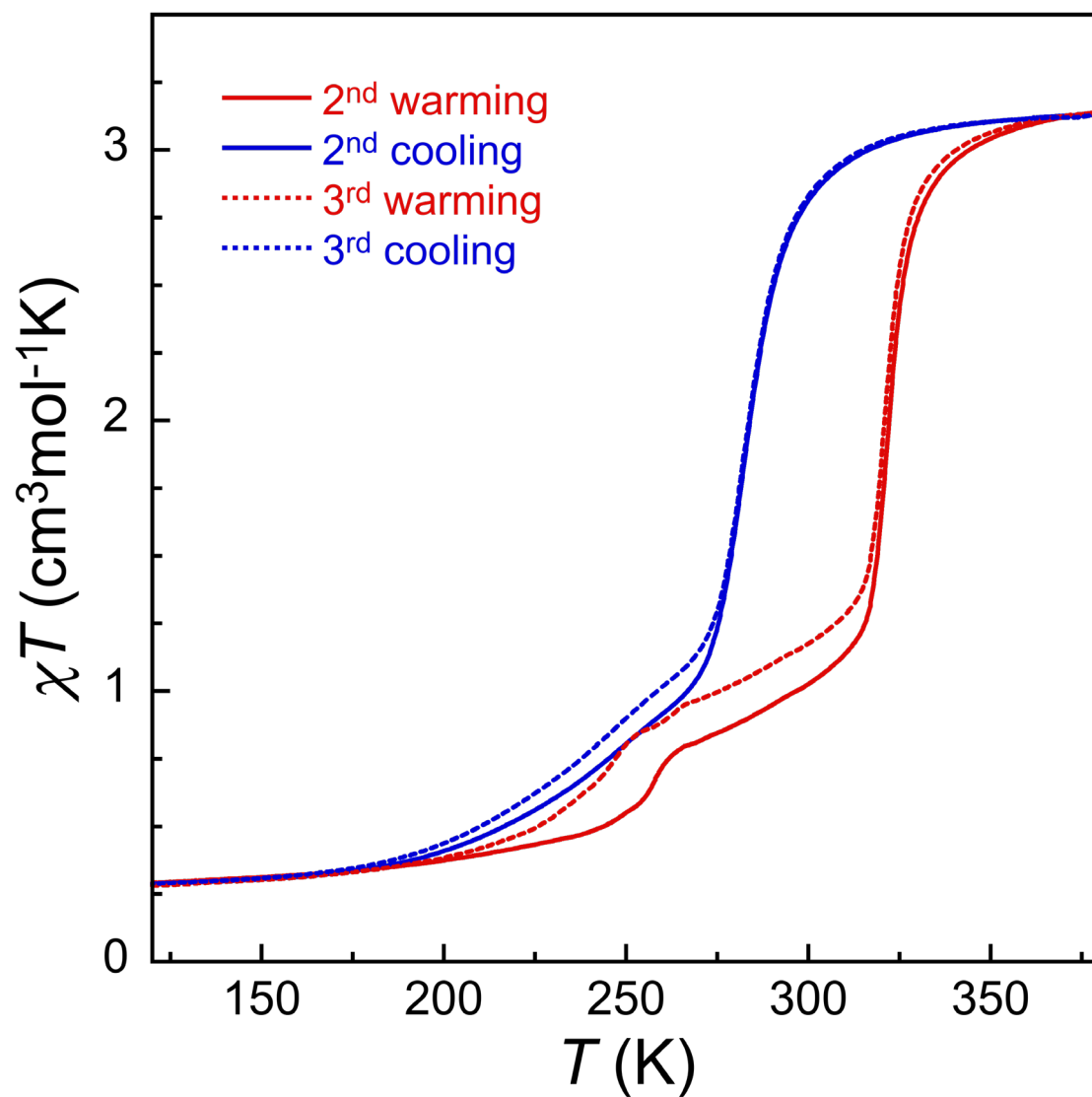


Figure S11. Reproducibility of SCO upon successive cycles. Variable temperature dc magnetic susceptibility ($\chi = M/H$ per mole of compound) data collected under an applied field of 0.5 T at 3 K/min, showing two successive thermal scans for the second batch of **1**, as indicated.

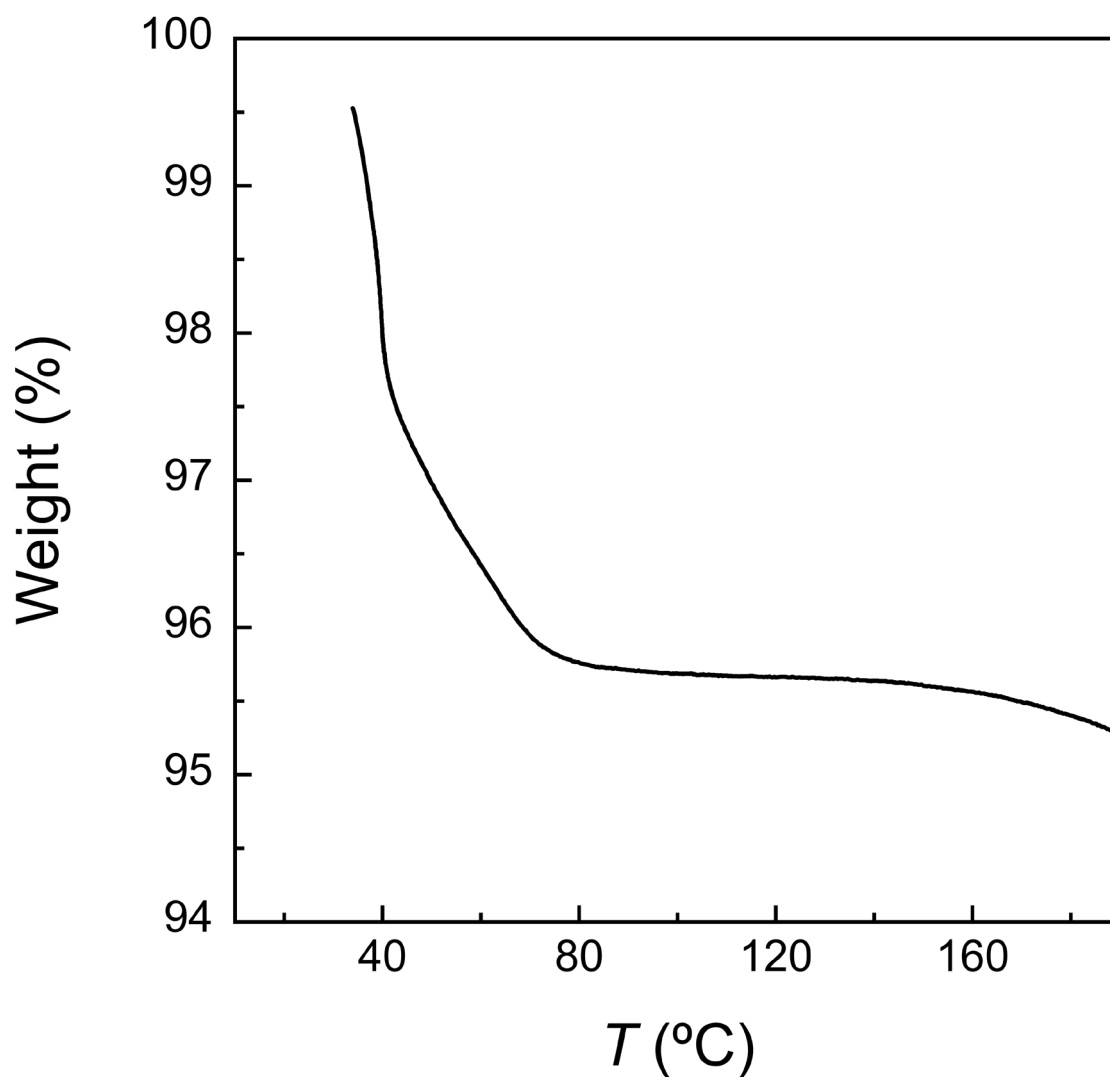


Figure S12. Thermogravimetric data for a polycrystalline sample of **1** exposed to air. The initial mass was 7.03 mg, and the sample already had lost some weight at the beginning of the measurement, *i.e.* after closing the oven and stabilizing temperature and air flow. The weight loss of *ca.* 4.3 % occurring below 80 °C would correspond to *ca.* 2 molecules of water per formula unit, likely absorbed upon exposure to air moist and very loosely bound to the solid. The further decrease in weight above 160 °C likely corresponds to the beginning of decomposition.

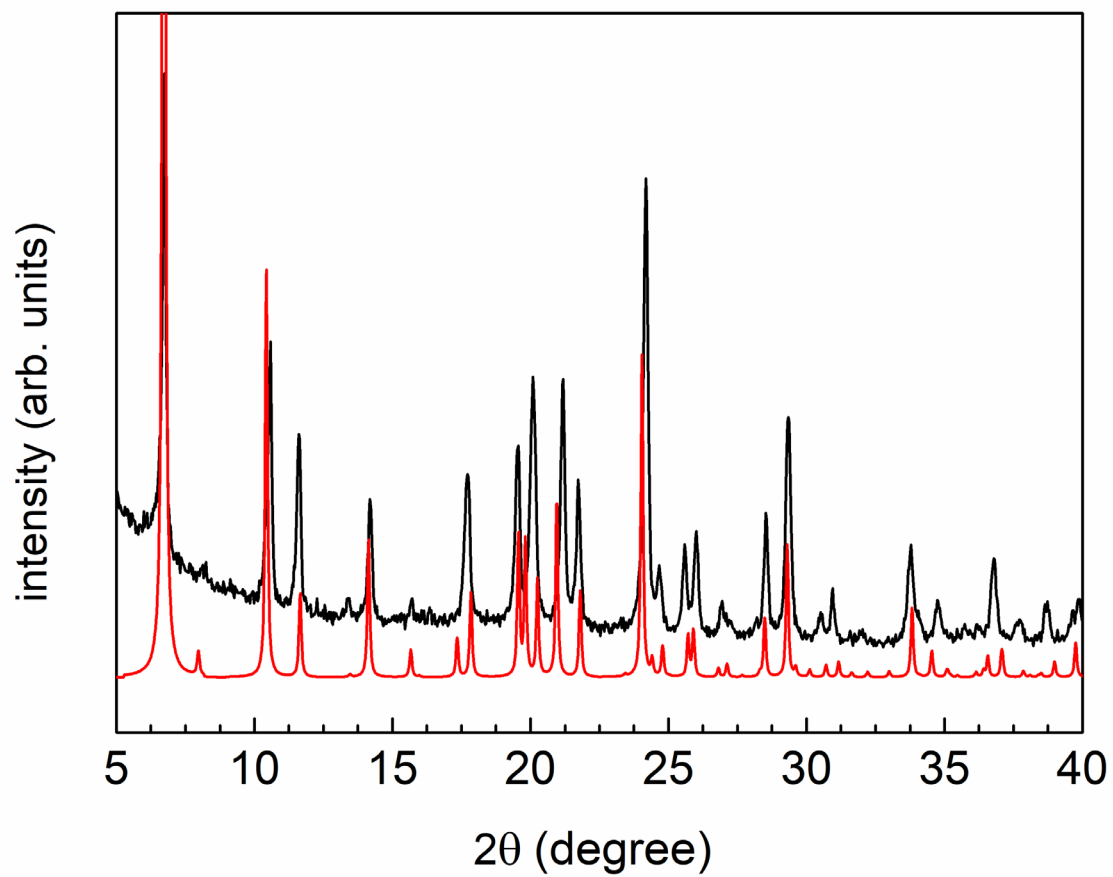


Figure S13. Powder X-ray diffraction pattern of **1** (black) compared to the pattern obtained from the crystal structure at 280 K (red).

Table S4. Crystallographic and refinement parameters for the structures of compound **2**

<i>T</i> (K)	100	200	275	300
Formula	8(C ₃₉ H ₃₀ FeN ₁₂), 3(FeCl ₄), 13(BF ₄), 23(C ₃ H ₆ O)			
FW (g mol ⁻¹)	8838.1			
Wavelength (Å)	0.7288			
Crystal system	monoclinic			
Space group	<i>C</i> 2/ <i>c</i>			
<i>a</i> (Å)	40.868(4)	41.41(2)	41.02(4)	41.317(8)
<i>b</i> (Å)	38.826(4)	39.35(2)	39.04(2)	39.303(8)
<i>c</i> (Å)	32.701(3)	33.45(2)	33.58(2)	33.740(7)
α (°)	90			
β (°)	128.243(3)	128.243(10)	127.471(4)	127.48(3)
γ (°)	90			
<i>V</i> (Å ³)	40753(7)	42818(41)	42681(53)	43478(21)
<i>Z</i>	4			
ρ_{calcd} (g cm ⁻³)	1.440	1.370	1.375	1.350
μ (mm ⁻¹)	0.593	0.596	0.612	0.624
indep. reflns. (<i>R</i> _{int})	43246 (0.0274)	29962 (0.0571)	18873 (0.0945)	18464 (0.0662)
parameters / restraints	3725 / 5478	3447 / 5195	2378 / 651	2270 / 486
GOF on <i>F</i> ²	1.045	1.111	1.003	1.039
<i>R</i> ₁ / <i>wR</i> ₂ [<i>I</i> > 2σ(<i>I</i>)]	0.0905 / 0.2491	0.1214 / 0.2929	0.0852 / 0.2337	0.0718 / 0.2036
<i>R</i> ₁ / <i>wR</i> ₂ (all data)	0.1071 / 0.2672	0.1363 / 0.2989	0.1052 / 0.2496	0.0975 / 0.2245
largest diff. peak / hole (e Å ⁻³)	1.591 / -1.498	0.835 / -0.694	0.591 / -0.531	0.648 / -0.964

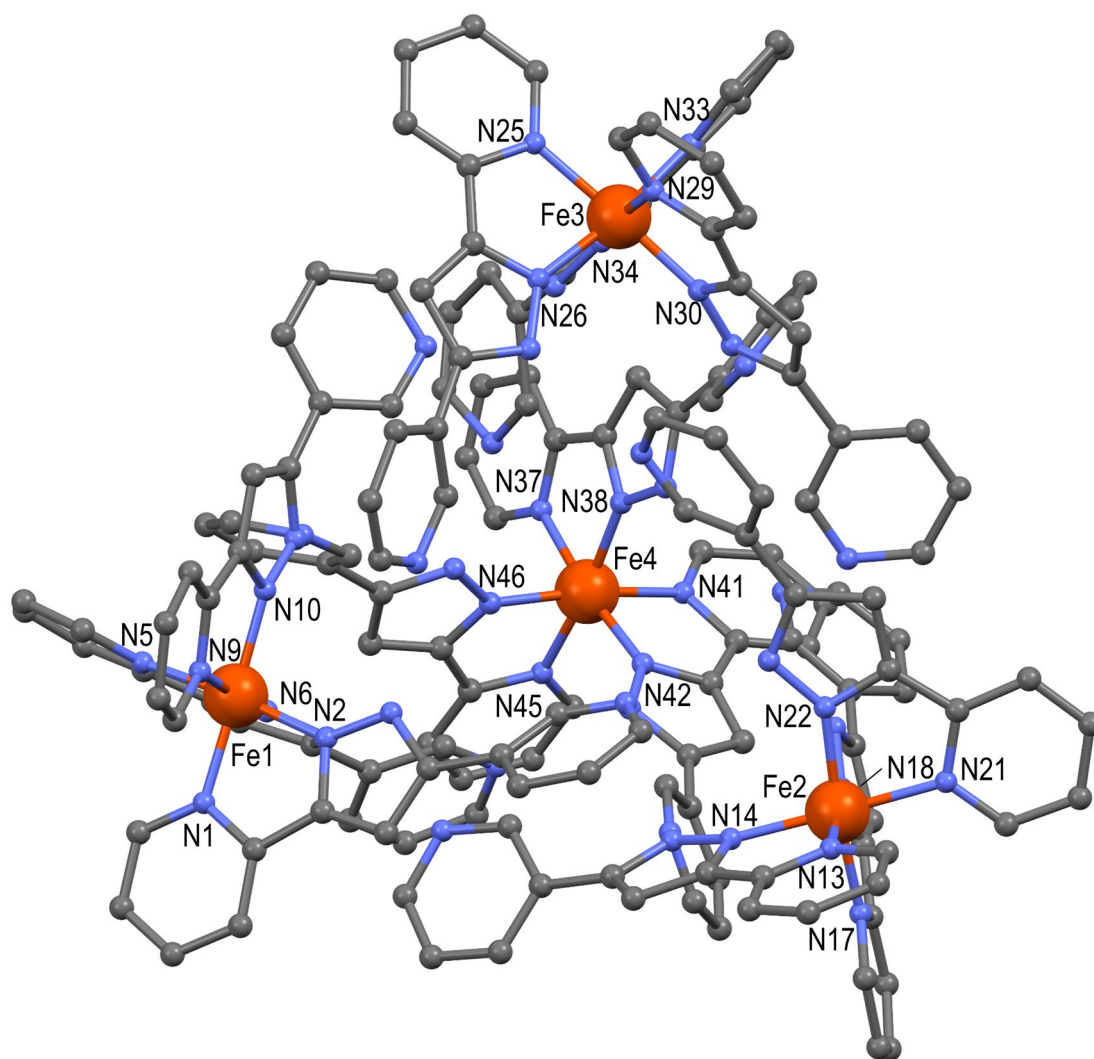


Figure S14. Representation of the $\{[\text{Fe}(\text{HL})_3]_4\}^{8+}$ cationic supramolecular tetrahedron of **2** at 100 K. Fe, N, and C atoms are shown in orange, blue and grey, respectively. H atoms are omitted for clarity. Only one disorder position is shown.

Table S5. Details of hydrogen bonds among the four $[\text{Fe}(\text{HL})_3]^{2+}$ complexes forming the supramolecular tetrahedron in the structure of **2** at 100, 200, 275 and 300 K. In the former two, only one set of hydrogen bonds is given for the two complexes disordered over two positions.

T (K)	D–H...A	D–H (Å)	H...A (Å)	D...A (Å)	D–H...A ($^\circ$)
100	N3–H3A...N28	0.88	2.07	2.85(3)	146.1
	N7–H7A...N16	0.88	2.04	2.816(5)	147.4
	N11–H11A...N48	0.88	2.00	2.749(19)	141.9
	N15–H15B...N44	0.88	2.08	2.884(12)	150.6
	N19–H19A...N32	0.88	2.29	3.083(15)	150.0
	N23–H23B...N4	0.88	2.00	2.776(5)	147.0
	N27–H27B...N24	0.88	2.11	2.908(12)	149.6
	N31–H31A...N40	0.88	2.05	2.792(16)	141.2
	N35–H35A...N12	0.88	1.82	2.606(10)	147.0
	N39–H39E...N20	0.88	2.29	3.075(11)	149.3
	N43–H43B...N8	0.88	2.05	2.800(8)	143.0
	N47–H47A...N36	0.88	1.97	2.722(14)	143.2
200	N3–H3A...N28	0.88	2.04	2.81(5)	144.7
	N7–H7A...N16	0.88	2.08	2.853(9)	146.4
	N11–H11A...N48	0.88	1.95	2.73(3)	146.9
	N15–H15B...N44	0.88	2.18	2.97(3)	149.6
	N19–H19A...N32	0.88	2.19	2.97(3)	147.4
	N23–H23B...N4	0.88	2.06	2.830(10)	146.4
	N27–H27B...N24	0.88	2.24	2.96(3)	138.8
	N31–H31A...N40	0.88	1.98	2.68(3)	136.2
	N35–H35A...N12	0.88	1.96	2.75(3)	149.8
	N39–H39E...N20	0.88	2.22	2.97(3)	143.3
	N43–H43B...N8	0.88	2.11	2.86(2)	142.2
	N47–H47A...N36	0.88	1.82	2.51(2)	133.3
275	N3–H3B...N44	0.86	2.08	2.822(8)	143.5
	N7–H7B...N20	0.86	2.11	2.857(8)	145.2
	N11–H11B...N32	0.86	2.05	2.806(8)	146.2
	N15–H15G...N12	0.86	2.08	2.841(8)	147.4
	N19–H19A...N48	0.86	2.05	2.806(8)	146.6
	N23–H23B...N36	0.86	2.09	2.799(8)	139.4
	N27–H27B...N4	0.86	2.08	2.816(8)	142.7
	N31–H31A...N16	0.86	2.07	2.822(9)	146.4
	N35–H35A...N40	0.86	2.07	2.800(8)	142.5
	N39–H39B...N24	0.86	2.10	2.853(8)	145.7
	N43–H43B...N28	0.86	2.07	2.797(8)	142.5
	N47–H47A...N8	0.86	2.09	2.847(8)	146.1
300	N3–H3B...N44	0.86	2.11	2.853(10)	144.7
	N7–H7B...N20	0.86	2.11	2.868(9)	146.6
	N11–H11B...N32	0.86	2.08	2.833(10)	145.8
	N15–H15G...N12	0.86	2.09	2.851(10)	147.7
	N19–H19A...N48	0.86	2.06	2.815(10)	146.3
	N23–H23B...N36	0.86	2.08	2.790(10)	140.1
	N27–H27B...N4	0.86	2.11	2.845(10)	143.5
	N31–H31A...N16	0.86	2.06	2.814(10)	146.5
	N35–H35A...N40	0.86	2.08	2.825(10)	144.0
	N39–H39B...N24	0.86	2.10	2.861(10)	146.9
	N43–H43B...N28	0.86	2.07	2.828(10)	146.0

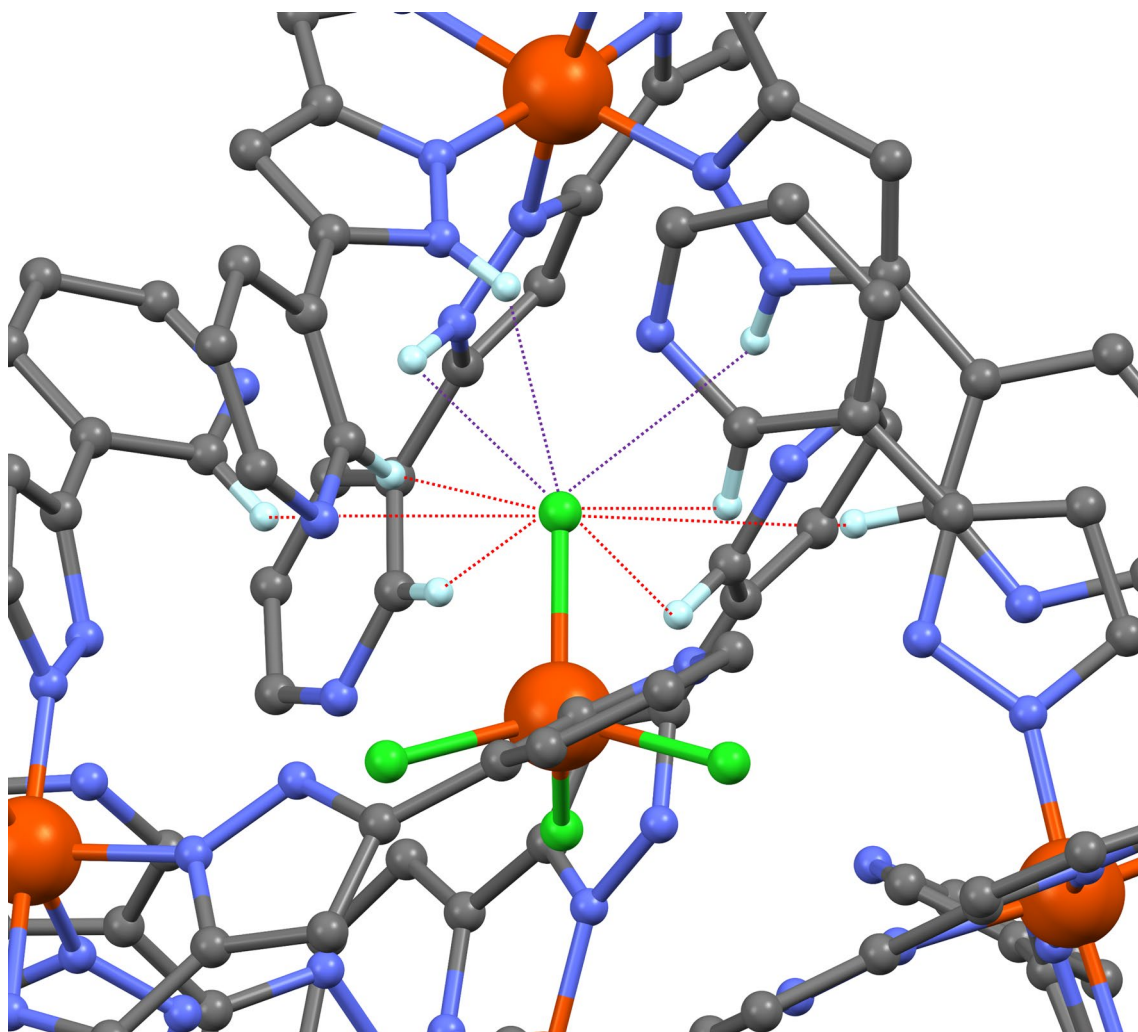


Figure S15. Selected area of the $[\text{FeCl}_4]@[\{\text{Fe}(\text{HL})_3\}_4]^{7+}$ cationic supramolecular tetrahedron of **2** at 100 K showing the H-bonding generated by the chloride ligands of $[\text{FeCl}_4]^-$. N–H...Cl and C–H...Cl interactions are shown as purple and red dashed lines, respectively. Fe, N, C, and H atoms are shown in orange, blue, grey, and white, respectively. H atoms that do not participate in the H-bonding are omitted for clarity.

Table S6. Range of short interactions of complex **2** at 100 K between the chloride ligands of $[\text{FeCl}_4]^-$ and the pyrazolyl NH and ortho CH pyridyl groups.

	N-H...Cl	C-H...Cl
Cl1	2.91–2.96	3.06–3.24
Cl2	2.73–3.01	2.83–3.31
Cl3	2.89–3.12	2.94–3.24
Cl4	2.89–2.96	3.04–3.25

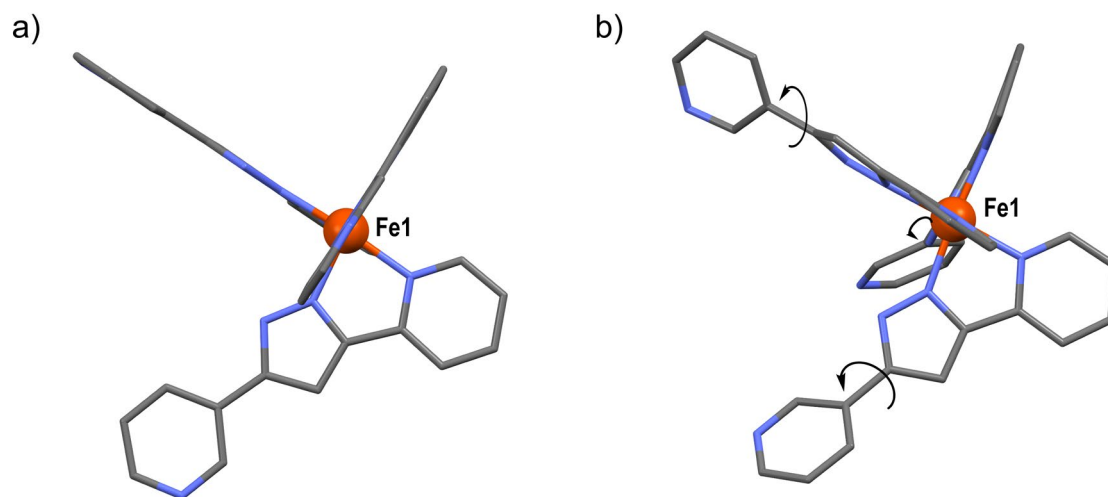


Figure S16. Representation of the $[\text{Fe}(\text{HL})_3]^{2+}$ cationic unit in compound **1** (a) and compound **2** (b). For compound **2**, Fe1 has been selected to evidence the rotation of the pyridyl external groups. Fe, N and C atoms are shown in orange, blue and grey, respectively. H atoms are omitted for clarity.

Table S7. Bond lengths (Å) describing the coordination environment of the Fe(II) ions in the structures of compound **2**.

<i>T</i> (K)	100	200	275	300
Fe1–N1	1.991(3)	2.016(7)	2.009(6)	2.048(8)
Fe1–N2	1.949(3)	1.977(6)	2.004(6)	2.026(7)
Fe1–N5	1.995(3)	2.016(7)	2.017(6)	2.060(7)
Fe1–N6	1.955(3)	1.975(7)	2.010(5)	2.037(6)
Fe1–N9	2.000(3)	2.030(7)	2.043(6)	2.057(7)
Fe1–N10	1.958(3)	1.964(6)	1.996(5)	2.023(6)
<Fe1–N>	1.975(18)	1.996(40)	2.013(34)	2.042(41)
Fe2–N13	1.989(4)	2.002(8)	2.028(6)	2.047(7)
Fe2–N14	1.966(4)	1.974(6)	1.972(6)	2.021(7)
Fe2–N17	1.998(6)	2.001(8)	2.035(6)	2.042(7)
Fe2–N18	1.971(4)	1.994(7)	1.967(5)	1.982(6)
Fe2–N21	2.010(4)	2.027(7)	2.005(7)	2.031(8)
Fe2–N22	1.964(5)	1.992(8)	1.972(6)	1.998(7)
<Fe2–N>	1.983(27)	1.998(44)	1.997(36)	2.020(42)
Fe3–N25	1.999(9)	2.079(19)	2.188(7)	2.197(7)
Fe3–N26	1.966(8)	2.08(2)	2.124(5)	2.133(7)
Fe3–N29	2.011(11)	1.98(2)	2.177(6)	2.192(7)
Fe3–N30	1.963(10)	2.050(18)	2.125(6)	2.145(7)
Fe3–N33	2.017(7)	2.098(17)	2.169(7)	2.193(8)
Fe3–N34	1.955(8)	2.03(2)	2.125(6)	2.127(7)
<Fe3–N>	1.985(53)	2.053(114)	2.151(37)	2.165(44)
Fe13–N125	1.991(10)	2.03(2)		
Fe13–N126	1.961(11)	1.92(3)		
Fe13–N129	2.013(10)	2.06(2)		
Fe13–N130	1.947(13)	1.984(19)		
Fe13–N133	2.006(9)	1.997(19)		
Fe13–N134	1.972(9)	1.94(2)		
<Fe13–N>	1.982(62)	1.989(128)		
<Fe3/13–N>	1.983(115)	2.021(128)		
Fe4–N37	2.022(8)	2.03(2)	2.019(7)	2.022(7)
Fe4–N38	1.959(8)	1.966(15)	1.963(5)	1.968(7)
Fe4–N41	1.993(7)	2.022(16)	2.006(6)	2.004(8)
Fe4–N42	1.954(8)	1.985(18)	1.943(6)	1.955(7)
Fe4–N45	1.995(7)	2.000(14)	2.011(7)	1.998(8)
Fe4–N46	1.979(8)	1.97(2)	1.969(6)	1.971(7)
<Fe4–N>	1.984(46)	1.996(103)	1.985(37)	1.986(44)
Fe14–N137	1.974(8)	1.973(18)		
Fe14–N138	1.959(8)	1.963(18)		
Fe14–N141	2.002(8)	2.019(19)		
Fe14–N142	1.939(9)	1.936(17)		
Fe14–N145	1.994(7)	2.009(15)		
Fe14–N146	1.955(9)	1.97(2)		
<Fe14–N>	1.971(49)	1.978(107)		
<Fe4/14–N>	1.977(95)	1.987(210)		

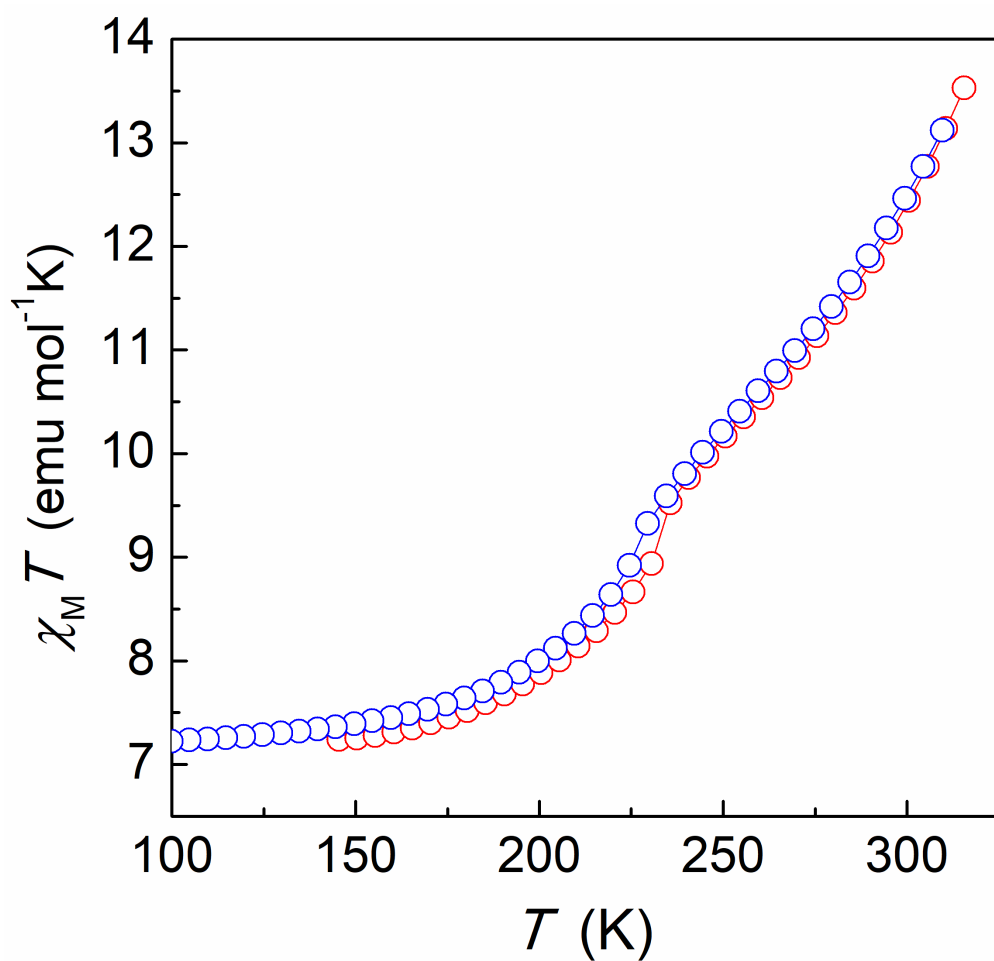


Figure S17. Variable temperature dc magnetic susceptibility ($\chi = M/H$ per mole of compound) data for fresh solvated crystals of **2** initially sealed within a polypropylene bag with a small amount of their mother acetone solution. The data was collected under an applied field of 0.5 T and is shown from 100 to 325 K. The cooling and heating modes are shown as blue and red circles, respectively.

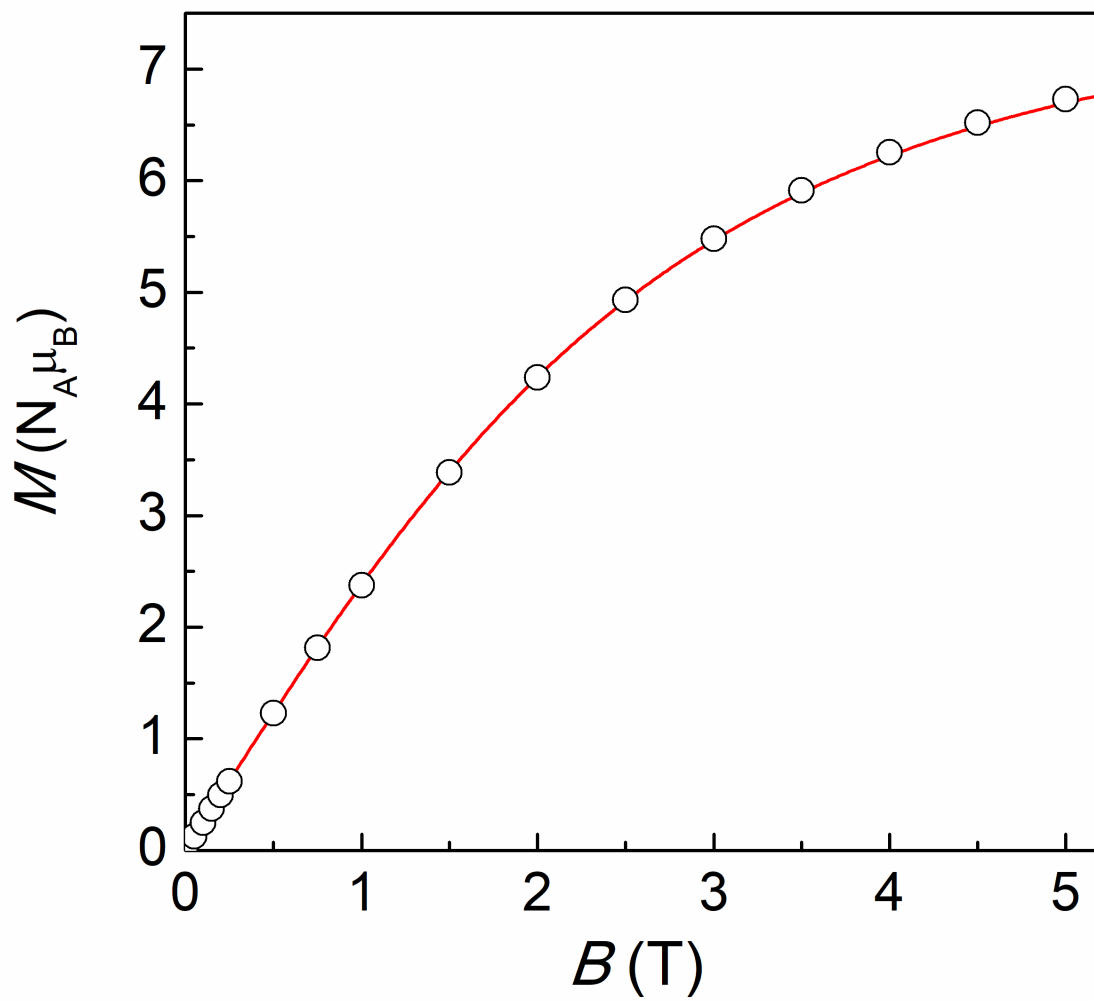


Figure S18. Magnetization vs. field data obtained at 5 K. The red line is the Brillouin function for 1.5 centers of $S = 5/2$ and $g = 2.06$.

Table S8. Stretching (ζ), angular (Σ) and torsional (Θ) distortions parameters for iron centres of compounds **1** and **2** at selected temperatures.

<i>Compound</i>	<i>Temperature (K)</i>	<i>Iron centre</i>	ζ (Å)	Σ (°)	Θ (°)
1	100	Fe1	0.1094	59.89	197.3
	280	Fe1	0.1619	80.94	258.6
2	100	Fe1	0.1247	66.35	200.4
		Fe2	0.0955	60.86	195.5
		Fe3	0.1479	61.20	201.5
		Fe13	0.1302	71.35	218.0
		Fe4	0.1154	60.55	194.8
		Fe14	0.1158	64.19	201.4
	200	Fe1	0.1454	68.18	203.9
		Fe2	0.0712	59.04	194.2
		Fe3	0.1860	74.22	225.4
		Fe13	0.2431	63.87	193.3
		Fe4	0.1307	62.82	186.2
		Fe14	0.1405	62.74	198.0
	275	Fe1	0.0643	63.18	207.0
		Fe2	0.1583	62.60	203.3
		Fe3	0.1593	88.29	279.7
		Fe4	0.1579	67.69	207.6
	300	Fe1	0.0788	67.72	220.5
		Fe2	0.1208	64.47	211.0
		Fe3	0.1752	91.25	288.2
		Fe4	0.1299	65.65	205.2

[1] L. A. Barrios, R. Diego, M. Darawsheh, J. I. Martínez, O. Roubeau, G. Aromí, *Chem. Commun.* 2022, **58**, 5375–5378.

[2] J. Harada, N. Yoneyama, S. Yokokura, Y. Takahashi, A. Miura, N. Kitamura and T. Inabe, *J. Am. Chem. Soc.*, 2018, **140**, 346–354.

[3] J. Juanhuix, F. Gil-Ortiz, G. Cuni, C. Colldelram, J. Nicolas, J. Lidon, E. Boter, C. Ruget, S. Ferrer and J. Benach, *J. Synchr. Rad.*, 2014, **21**, 679–689

[4] G. M. Sheldrick, *Acta Cryst. A*, 2015, **71**, 3–8.

[5] G. M. Sheldrick, *Acta Cryst. C*, 2015, **71**, 3–8.

[6] G. M. Sheldrick, 2012, *SAINT and SADABS*, Bruker AXS Inc., Madison, Wisconsin, USA.

[7] A. L. Spek, *Acta Cryst. C*, 2015, **71**, 9-18.